

Article

Not peer-reviewed version

Effect Of Tendon Profile Layout On Flexural Strength Of Unbounded Post-tensioned Prestressed Concrete Bridge I-Girder

[Swar Imad Hasib](#) ^{*}, [Assim Mohammed Lateef](#), Omar Oarani Aziz

Posted Date: 25 February 2025

doi: 10.20944/preprints202502.1963.v1

Keywords: tendon profile; flexural strength; unbounded; post-tension; prestress; bridge; ultimate load; cost



Preprints.org is a free multidisciplinary platform providing preprint service that is dedicated to making early versions of research outputs permanently available and citable. Preprints posted at Preprints.org appear in Web of Science, Crossref, Google Scholar, Scilit, Europe PMC.

Copyright: This open access article is published under a Creative Commons CC BY 4.0 license, which permit the free download, distribution, and reuse, provided that the author and preprint are cited in any reuse.

Article

Effect of Tendon Profile Layout on Flexural Strength of Unbounded Post-Tensioned Prestressed Concrete Bridge I-Girder

Swar I. Hasib ^{1*}, Assim M. Lateef ¹ and Omar Q. Aziz ²

¹ Department of Civil Engineering, Tikrit University, Tikrit, Salah-Al Din, Iraq; assaim77@tu.edu.iq

² Department of Civil Engineering, University of Salahaddin, Erbil, Kurdistan Region, Iraq; Omar.Qarani@su.edu.krd

* Correspondence: sewar.imad@st.tu.edu.iq; Tel.: +9647702188806

Abstract: The main objective of this research is to evaluate the optimal design of the tendon profile layout and to examine the effect of the tendon profile layout on the flexural strength of unbounded post-tensioned prestressed concrete bridge I-girders. In this study, the experimental investigation involved casting and testing ten unbounded post-tensioned bridge girders under a four point loads. The main variable studied was the tendon profile layout. The experimental results showed that the flexural behavior of tested specimens is divided into three stages: elastic stage, elastic-plastic stage and plastic stage and all specimens exhibit flexural failure. It can be concluded that for each tendon profiles layout (trapezoidal, parabolic, harped), the tendon profiles with eccentricity at end of beam ($e_e=0$), had maximum ultimate load capacity. It also can be concluded that specimen GF-9 HA (Harped Tendon Profile with $e_e = 0$ mm) had maximum ultimate load capacity from all other specimens. These enhancement in specimens stiffness, ultimate loads capacities and deflections because of increasing resisting capacity, reducing stresses specially at support, reducing deflection, increasing resisting bending moment which lead to reducing the production cost of girder.

Keywords: tendon profile; flexural strength; unbounded; post-tension; prestress; bridge; ultimate load; cost

1. Introduction

Modern structural engineering has been moving towards more economical structures by continuously improving design methods and using higher strength materials. This results in smaller cross sectional area and hence weight reduction. Especially for reinforced concrete, where dead loads represent a large amount of load, such advancements are vitally important. Prestressed concrete were developed to overcome the limiting features of ordinary reinforced concrete.

The prestressing systems are defined as the preloading of a structure, prior to service loads application to improve structure performance in a specific way. The prestressing concrete systems include two types of prestressing. The first type is called pre-tensioning prestressing (the tendons are stressed before concrete is placed), and the second one is known as post-tensioning prestressing (the tendons are tensioned after concrete is placed) [1–3]. In bridge construction, the post-tensioned concrete system is most commonly used, as it has much better advantages compared to the traditional reinforced concrete. This system offers improved material utilization, enhanced deflection and crack control, increased durability, faster construction times, reduced costs, and greater design flexibility [4].

A typical post tensioning tendon includes prestressing strands, ducts that house the strands, grout and anchorages that transfer the forces to the concrete [5].

There are two ways to achieve post-tensioned prestressed concrete: bonded post-tensioning and unbonded post-tensioning. In bonded post-tensioning the tendons are in direct contact with the

surrounding concrete, transferring stresses through bond at the surface. On the other hand, in unbonded post-tensioning, tendons are away from the concrete, so the stress is not transferred through bonding of the surface. The profile of the tendon is important for decreasing the tensile stress in the concrete. Finally, forces induced by the curvature of the tendons provide the counterbalancing forces which compensate the tensile forces induced by applied load. In order to counteract sagging bending moments caused by the transverse loads, tendons are positioned with eccentricities toward the soffit of the beam. When the prestressing force is applied the prestressed beam deflect upward. The profile of bending moment diagram is equal to tendon profile layout because the bending moment diagram represent the product of eccentricity and prestressing force [6].

Flexural strength indicates the tensile strength, or ability for a beam or slab to resist bending moments up to the point where failure occurs [7].

In recent decades, numerous experimental and numerical studies have been conducted to examine the flexural behavior of unbonded prestressed concrete beams. Additionally, several numerical investigations have explored the impact of tendon profile configurations on the overall structural performance. Tang et al. in their study, they examines the flexural performance of prestressed concrete bridge girders through experiments and Finite element modeling, providing insights into capacity, failure mechanisms, and design recommendations for engineers [8]. Moreira et al. in their research, a finite element simulation of unbonded prestressed concrete beams was conducted, and a convergence method utilizing the Newton-Raphson scheme was developed for this purpose [9].

Páez et al. in their study, a long term pretension loss analytical method was provided, and new formulas for the long term prestress loss were developed [10]. Kim et al. in their study, eleven test specimens of post-tensioned prestressed concrete beams with different strength strands were used to evaluate the flexural performance. The results showed that the increase in stress in the high strength strands was underestimated by ACI 318-19 [11] and AASHTO [12] design criteria [13]. Najem in his study, the best section design was done only considering flexural design constraints, including limiting the maximum stress at the extreme fibers of the section, which in turn were included in the design criteria. Another change implemented to the solution was to determine the variable tendon eccentricity's optimal location along the beam's longitudinal section. Also, tendon placement needs to be subject to certain design constraints concerning geometry and other design limitations. They ensure that the optimal placement of the tendon neither interferes with nor violates the original design integrity of the post-tensioned beam [14]. Park et al. in their work a total of five large post-tensioned beams were tested to examine flexural behavior with high-strength strands concerning concrete compressive and strand tensile strengths. Results matched code predictions, showing similar crack patterns and ductile behavior. Minimal excess in crack widths and stresses occurred under service loads, controllable with proper deformed rebar arrangement [15]. Dogu et al. provided a method to predict the flexural behavior of post-tensioned ultra-high performance concrete (UHPC) beams with unbonded tendons is introduced. It uses a mechanics-based model to determine ultimate strand stress based on neutral axis depth, tendon properties, loading, and strains. Considering fiber tension and UHPC compression failure modes, predictions for 221 beams showed less than 5% accuracy and a coefficient of variation less than 17% [16]. Oukaili et al. provided a nonlinear analysis to developed two models to predict partially prestressed concrete flexural members with unbonded strands. One model used FORTRAN, the other ABAQUS. Validated with 22 beams and slabs varying in concrete strength, jacking stress, prestressing index, and span-to-depth ratio. Models accurately predicted cracking loads, ultimate resistance, deflection, and strain, matching experimental data [17]. Vichare et al. studied an efficient methodology for analyzing and designing prestressed concrete bridges using CSi Bridge software. It simplifies complex modeling by handling dead loads, prestress forces, and live loads effectively. Results demonstrate CSi Bridge's automation capabilities, the dominance of dead loads in flexural design, live loads in shear, and the crucial role of cable profile positioning for stability and efficient design [18]. Aravinthan et al. provide an experimental study examined the flexural behavior of single and two-span continuous beams with highly eccentric

tendons. Variables included tendon profiles, loading patterns, casting methods, and confinement reinforcements. Results showed similar flexural responses across tendon layouts, increased ductility from confinement without raising ultimate strength, and tendon layout and loading patterns affected moment redistribution [19]. Ibrahim et al. studied the flexural behavior of corrosion-damaged reinforced concrete slabs reinforced with carbon fiber-reinforced polymer (CFRP) using NSM and CFRP strips. Slabs experienced 11%, 26%, and 40% corrosion. CFRP strengthening restored and surpassed original capacities, significantly enhancing yield strength. However, at 40% corrosion, yield strength declined, reducing load capacity strengthening from 38% to 15% [20]. Khalid Khdir et al. studied evaluates the flexural behavior of prestressed Ultra High Performance Concrete beams, a modern concrete type gaining popularity for its high compressive and tensile strength, toughness, and durability. Four prestressed beams with compressive strengths from 40 MPa to 160 MPa, a reinforcement ratio of 0.00465, and a d/b ratio of 1.536 were tested. Results indicated that increasing compressive strength enhanced the ultimate load by approximately 46%. Load-deflection curves remained linear up to the yield load, similar to normal concrete. Failure occurred through tensile fiber debonding and pull-out, due to the random distribution of fibers. Additionally, strains in unbounded tendons were incompatible with the adjacent concrete [21]. Burhan provided a finite element model to study creep, shrinkage, and tensile stiffness between cracks in partially prestressed continuous composite beams with deformable shear connections. The versatile algorithm accommodates any viscous law and load history. Numerical comparisons demonstrate its potential, and its simplicity allows easy implementation in analytical programs [22].

Ng et al. Stated that the profile determination of pre-stressed tendons stands as a vital component in post-tensioned concrete structure design. They stated that using the load balancing method provides substantial capabilities to obtain tendon profiles directly. They provided detailed explanations about method applications through two specific examples which showed step-by-step procedures in different conditions. The method proves easy to execute for complex structural elements including curved continuous bridges according to the examples presented. Tests demonstrate that the load balancing technique surpasses traditional approaches in efficiency so standard procedures should implement it according to research findings [23]. Ahmad Ali Khan et al. used finite element finite element to propose a tendon layout design for one-way pre-stressed concrete slabs. Her, they considered B-Spline for the tendon layout design for slabs. The stresses of the structural body were calculated with the finite element method. They modeled the tendons as parabolas and increased their eccentricities to minimize tensile stresses, despite the fact that the use of parabolas in design of cables is complicated, particularly for continuous structures in which tendons are nominally not parabolic. The ordinates of the B-Spline were modified in such a way that the overall shape of the tendons fitted the intended profile. As they designed the tendon layout, they verified that the stress in the structural components would not exceed the allowable maximum tensile stress. The tendon profile was then iteratively optimized according to the stress results from the finite element analysis [24]. Chaitanya Kumar et al. Applied a genetic algorithm based optimization method for the design of simply supported prestressed concrete beams subjected to live and dead loads. In order to minimize cost they considered a tendon to concrete cost ratio of 8. They studied factors including beam length, tendon profile, sizing of population in the algorithm, and live load intensity that are effective in optimizing cost. Results demonstrated increase of 21.7% in the optimum cost when beam length is increased from 14 m to 15 m and a 16.8% increase when live load is increased from 50 kN/m to 60 kN/m. Parabolic tendon profiles increase optimum cost over straight profiles by 4.22% for beam lengths of 14 m and 15 m [25]. Colajanni et al. explained the design procedures for pre-stressed beams made from pre-stressed concrete. They provided the optimal layout for standard reinforcement in pre-stressed concrete beams that are subjected to bending moments and shear forces[26]. Dixit et al. Investigated the effects of eccentricity, prestress load and tendon profile using a three dimension finite element model of a post-tensioned concrete beam under concentrated point loading. Analysis was done using the ANSYS program. Static analysis results indicated that parameters including eccentricity, prestress load, and tendon profile are vital

components in the design of post-tensioned concrete beams[27]. Naser studied the impact of the tendon profile on structural performance of post-tensioned concrete bridges in terms of moment bending, shear force, stress, and vertical deflection. The research studied two tendons profiles among multiple bridge models which are seven simply supported and ten continuous bridge models. Simulation using the Finite Element Method revealed that depending on the type and number of tendon anchorage points used, the performance of the bridges altered. In terms of serviceability loads, the continuous tendon profile design is preferred to be a post-tensioned concrete bridge solution as it follows a design that induces lower deflection in the vertical [28]. Mohammed et al. investigated the structural performance of post-tensioned two-way concrete slabs with diverse bonded tendon layouts. They investigated these tendon arrangements through a parametric study of slab tendon geometry and loads using non-linear finite element analysis. The results showed that the slab post-tensioned in both directions failed at a load approximately 89% greater than the slab post-tensioned only in one direction[29]. Zelickman et al in their work a new method of optimizing the post-tensioned cable layouts in concrete slabs using 3D B-splines is introduced. Exact prestressing forces are modelled as cables and projected onto finite element meshes. Advanced designs using spline control points reduce cable weight by more than 20% on regular floors, and over 50% on irregular layouts without compounding performance [30]. Xu et al. in their work, the impact of external prestressing tendons on reducing main span deflection and concrete stress was studied using finite element models. Analytical evaluations on steel and concrete beams assessed tendon contributions. An optimized tendon layout for hybrid beam rigid frame bridges was developed, considering long-term shrinkage, creep, and tensioning schemes for maintenance insights [31]. Usha Rani noted that the deflection of prestressed concrete beams with different cable profiles including straight tendons, parabolic tendons, parabolic tendons with eccentric anchors, trapezoidal tendons, sloping tendons, and parabolic and straight cable combinations is estimated. The analysis is performed using the basic concepts C programming and conditional if statements. The results of this method are compared with those obtained from an appropriate analytical method [32]. Mohamed et al studied the enhanced RC T-beams using external prestressing tendons to improve load capacity and resistance. Seven beams were tested under four-point loading: one strengthened and six with straight, V-shaped, or U-shaped tendons. Finite element analysis showed cracking, yield, and ultimate loads increased by up to 250%, 570%, and 30%. Straight tendons with deviators performed best[33].

The tendon profile layout is important factor in the design of post-tensioning concrete bridges but most studies that deal with tendons profile layout were studied the effects of tendons profile layout on the structural performance for prestressed concrete beams and slabs, numerically but experimental studies are not exist and if there is exist it is very little.

In this study, an experimental investigations were carried out to provide better understanding on the flexural behavior of unbonded posttensioned prestressed concrete bridge girders with different tendon profile layouts and eccentricities at end anchorages. Experiments were conducted on ten I-section simply support, of unbonded single-strand prestressed post-tensioned beams with various profile shapes and eccentricity at the end anchorages, that were designed according to ACI 318M-19. The rate of contribution of tendon profile layout were investigated on the improvement of :-

1. Increasing Load resistance.
2. Increasing of bending moment capacity.
3. Better deflection control.
4. Increasing the stiffness of prestressed concrete I-bridge girders.
5. Decrease in construction costs.

Finally, the ultimate capacity and serviceability observed through the tests, and some recommendations for the design and practical application of tendon profile layout of unbonded prestress concrete I-bridge girders are provided to engineers and designers.

2. Experimental Program

2.1. Size and Shape of the Test Specimens

In this study, ten I-section simply support prestress post-tension beams with various profile of unbonded single strand were designed according to ACI 318M-19 Code and used in experimental program [1,11,34,35]. All the beam were geometrically similar having dimensions 3300 (L) x 250 (W) x 500 (D) mm and solid (rectangular) end blocks were provided at the ends, as shown in Figure 1.

These end blocks serve to accommodate the necessary end anchorage hardware and provide supplemental reinforcement, they are little use in reducing transverse tension and avoiding cracking.

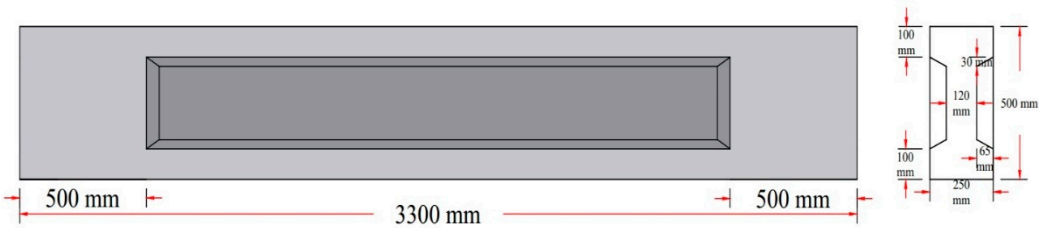


Figure 1. Dimension of Post-tensioned I-beam with rectangular end block.

2.2. Prestressing and Reinforcement Detail

In each of 10 tested specimens (beams), the main reinforcement was a single seven-wire low relaxation strand of 15.24 mm diameter (Grade 270) conforming to the requirement of ASTM A416/A416M standard specification for steel strand [36], were served as unbounded prestressing steel and was located in plastic duct of 20 mm inner diameter. Deformed steel bar are used of 12 mm diameter for longitudinal steel bars to hold the stirrups and 10 mm for vertical stirrups (all beams were designed for shear to avoid premature shear failure). Stirrups were spaced at 200 mm center to center along the beam, while

125 mm center to center spaced stirrups were used at the beam ends (anchorage zone) to prevent sudden shear failure and amplify end anchorage for the prestressed specimens. Figure 2 shows a reinforcement detail for Post-tensioned I-beam with end blocks.

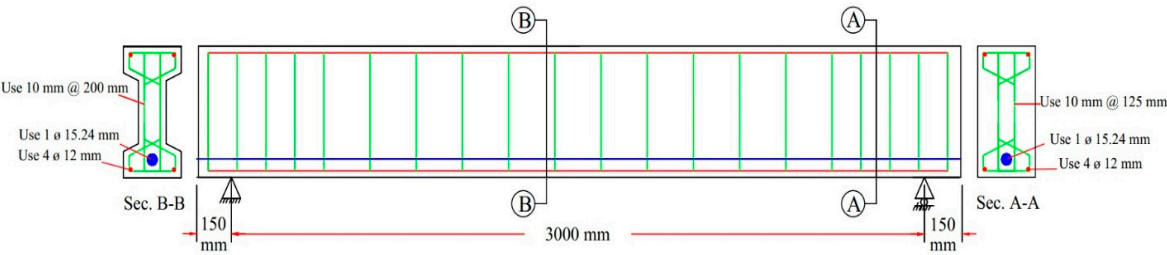


Figure 2. Reinforcement detail for Post-tensioned I-beam with end blocks.

The physical properties of strand and bares are summarized in Table 1.

Table 1. physical properties of strand and rebars.

Type	Diameter (mm)	Area (mm ²)	Yield stress (Mpa)	Ultimate Strength (Mpa)	Maximum Elongation (%)	Modulus Of Elasticity (Mpa)
strand	15.26	140.54	-	2018	4.28	196,370
Deformed bar	11.74	108.28	595	673	20	200,000
Deformed bar	9.857	76.31	610	696	21	200,000

2.3. Concrete Mix Specification

The concrete mix was designed based on the (ACI 211.1) Code, and performing the guides in (ACI 211.1R) Code [36]by using high performance super plasticizer admixture type Sika Visco Crete 1681, proportion of concrete mix was listed in Table 2. The compressive strength of cubes (f_{cu}) at 28 days not be less than 55 Mpa [37]

Table 2. Concrete mix proportion

Cement (g)	Water (L)	Additive (L)	Fine Aggregate (kg)	Coarse Aggregate (kg)	W/C	Slump (mm)	Maximum Aggregate Size (mm)
425	160	4	880	910	0.38	150-180	19

The compressive strength of concrete was determined from 150x150x150 mm cubic samples after 28 days of curing, and the average compressive strength (f_{cu}) results for 12 concrete cubes was 71.6 Mpa were tested by concrete compressive machine. The measured slump was 160 mm for job mix.

The splitting tensile strength was found by testing 150x300 mm cylindrical specimen according to ASTM C496/C496M standard as illustrated in Figure 3 (a) and splitting tensile strength (f_t) was 3.64 Mpa [38].

The flexural strength was obtained by testing 150x150x550 mm prisms as illustrated in Figure 3 (b). Using standard test method for flexural strength of concrete (using simple beam with third-point loading) according to ASTM C78/C78M and modulus of rupture (f_r) was 4.9 Mpa [39].

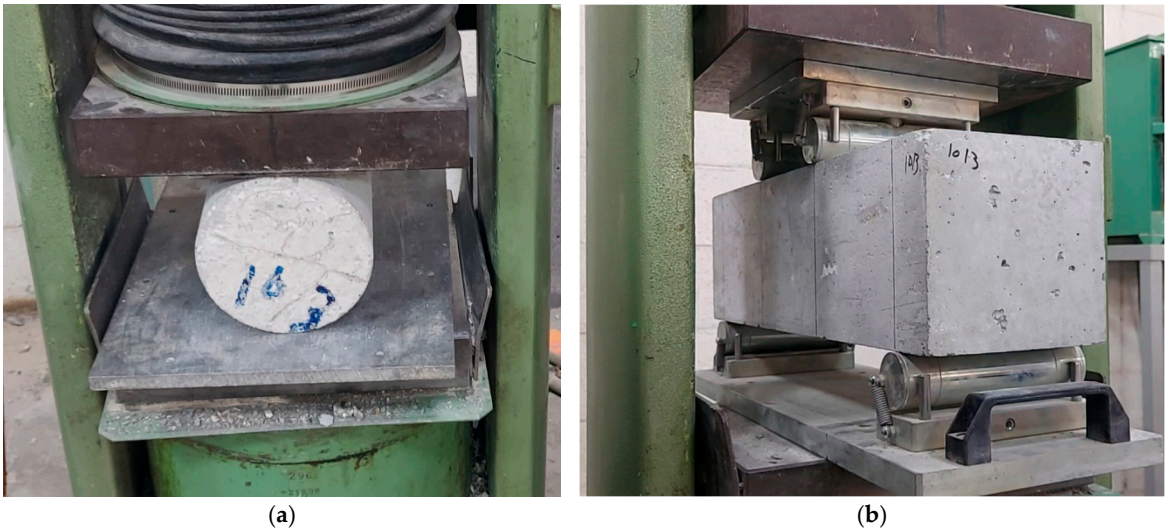


Figure 3. (a) Splitting tensile strength test. (b) Prism test.

The modulus of elasticity obtained using 150x300 mm cylinder in accordance to ASTM C469/C469M as illustrated in Figure 4 [40]. For measuring deformation a dial gauge of 0.001 mm accuracy was used and the modulus of elasticity (E_c) was 34699 Mpa.



Figure 4. Standard test for static modulus of elasticity.

2.4. Preparation of the Test Specimens

Reinforcement were prepared accurately as shown in Figure 5 (a). The strands were prepared at the factory, one strand were cut for each beam with a total length of 3.70 m and inserted into the plastic ducts of 20 mm inner diameter and these ducts were previously embedded inside the specimen body as shown in Figure 5 (b) and Spiral reinforcement was provided at end block (anchorage zone) as shown in Figure 5 (c).



Figure 5. Reinforcement preparation: (a) Beam reinforcements detail. (b) Strand in plastic duct. (c) Spiral reinforcement.

Special molds made from steel and plywood was used for reinforced beam casting in separate matching. Particularly, ten reinforced concrete beams were constricted at Kirkuk Limited Company for Concrete Girder as shown in Figure 6.

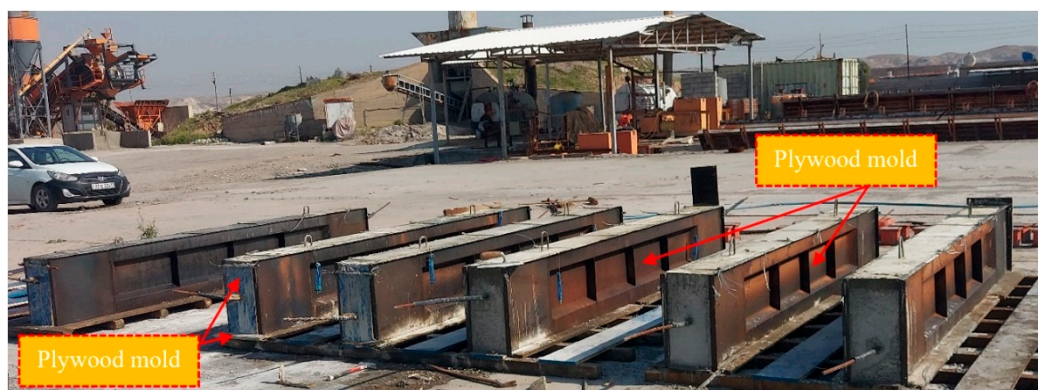


Figure 6. Special molds made from steel and plywood used casting for specimen.

After 28 days from casting (concrete placement), post-tensioning of the beam was performed by a skilled staff of the prestressing concrete plant. A post-tensioning machine was used as shown in Figure 7 (a). The strands were tensioned up to 0.7 ultimate strength (f_{pu}) to reach a full prestressed condition under full service load. At first, 20% of jacking force was applied to tighten the wedge and plate in accurate position, then a full jacking force of 182282 N was applied to the strand as shown Figure 7 (b).

The control of the jacking force was made by the load indicator of the hydraulic jack and by monitoring the elongation of the strand and the process of post-tensioning took approximately 15 min. for each beam.



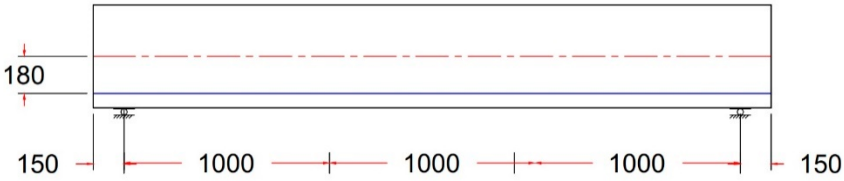
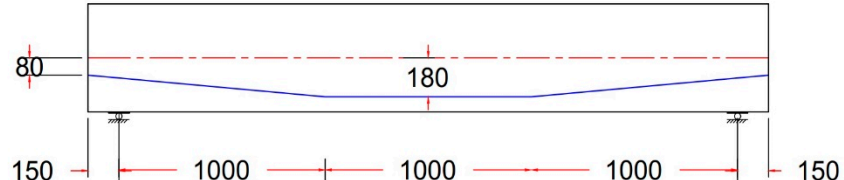
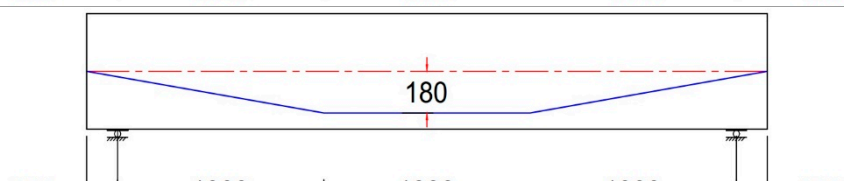
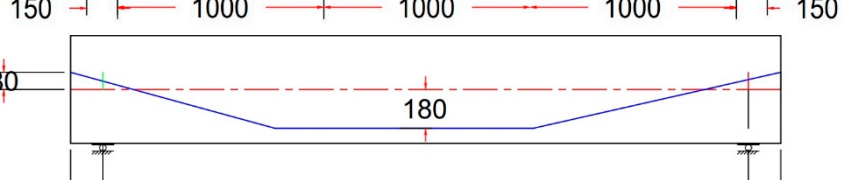
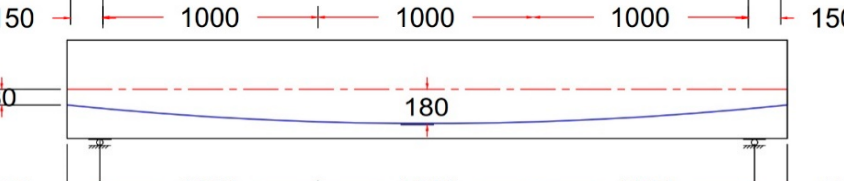
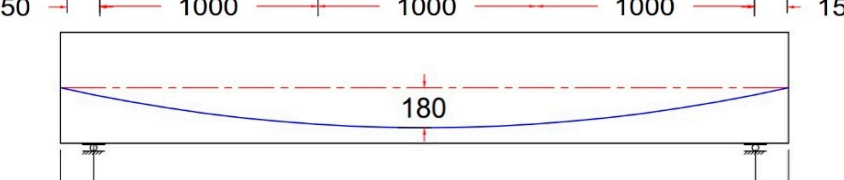
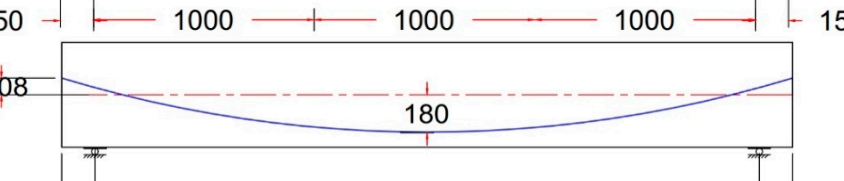
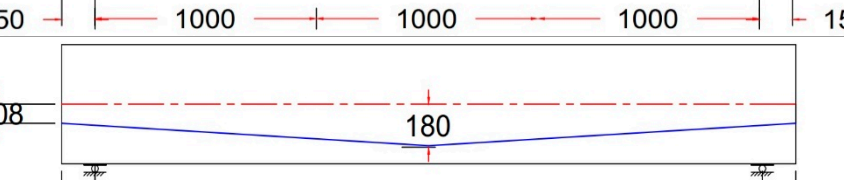
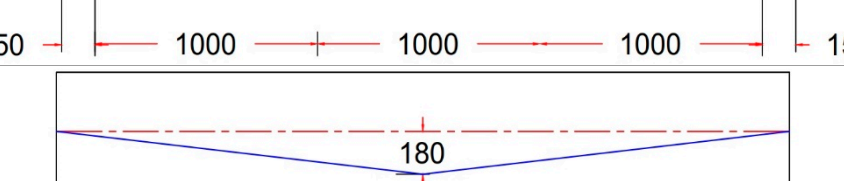
Figure 7. (a) Post-tensioning machine. (b) Applying post-tensioning force.

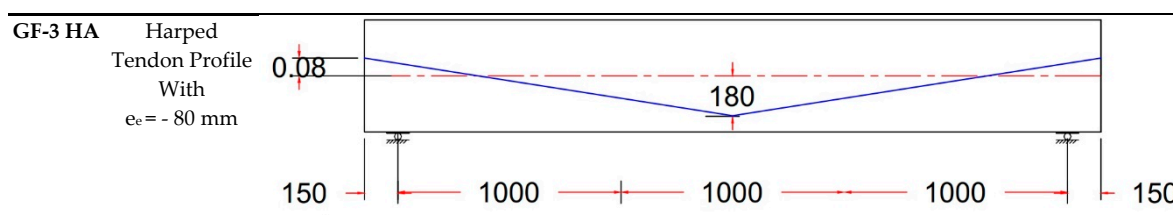
2.5. Experimental Variables

The options of selecting test variables were carefully studied, and specimens was prepared for most questionable parameter. The target variable was Tendon Profile Layout, ten prestressed reinforced concrete beams with different Tendon Profile Layout were constricted as illustrated in Table 3.

Eccentricity at mid-span was 180 mm for all beams, while it varies between (180 , 80 , 0 , -80) mm at anchorage points (at the end face of the beam).

Table 3. Specimens (Beams) with tendon profile layout.

Specimen name	Tendon Profile name	Tendon Profile layout, units in (mm)
GF-1 ST Control Beam	Straight Tendon Profile With $e_e = 180\text{ mm}$	
GF-2 TR	Trapezoidal Tendon Profile With $e_e = +80\text{ mm}$	
GF-3 TR	Trapezoidal Tendon Profile With $e_e = 0\text{ mm}$	
GF-4 TR	Trapezoidal Tendon Profile With $e_e = -80\text{ mm}$	
GF-5 PR	Parabolic Tendon Profile With $e_e = +80\text{ mm}$	
GF-6 PR	Parabolic Tendon Profile With $e_e = 0\text{ mm}$	
GF-7 PR	Parabolic Tendon Profile With $e_e = -80\text{ mm}$	
GF-1 HA	Harped Tendon Profile With $e_e = +80\text{ mm}$	
GF-2 HA	Harped Tendon Profile With $e_e = 0\text{ mm}$	



2.6. Test Setup and Instrumentation

Experimental tests were conducted at the Laboratory Of Civil Engineering , University Of Salaheddin-Erbil. Four points load test was carried out to investigate the flexural behavior of unbonded prestressed post-tensioned beam. Specimens were simply supported at both ends.

The tested machine was consisting of a steel frame, with capacity of 2500 KN as illustrated in Figure 9. Application of the load was performed through a hydraulic circular jack to a load cell with capacity 1000 KN, which used for measuring the load through the tests, and then to a load distributing steel beam. The load distributing steel beam was dividing the load into two regions (points) loading with distance 1000 mm between them , through two welded round bar (30 mm diameter) to the two plats(5mm thickness) putted below them . Finally the load was transferred to the concrete surface. Supports were consisting of rectangular (tube) steel section, braced against bending, distortion and restricted against horizontal movement. The clear span between two supports was 3000 mm. A 30 mm smooth bar was welded on the support with plate (5mm thickness) put in between the bar and the bottom of the beam, plates can rotate smoothly with rotation of the specimens at supports as illustrated in Figure 9.

Two Linear Variable Displacement Transducer (LVDTs) with gauge length 300 mm were used in this experiment to measure the center deflection of the beam as applied load increases. The LVDTs were placed in the mid-span of the beam attached to a rectangular steel tube which putted in between LVDTs and beam bottom face to obtain maximum displacement of the specimens (beams). First LVDT putted in the front face of the beam and the second one in the back face in midspan of the beam, so we can use the average displacement if the steel tube does not remain straight and becomes inclined as illustrated in figure.

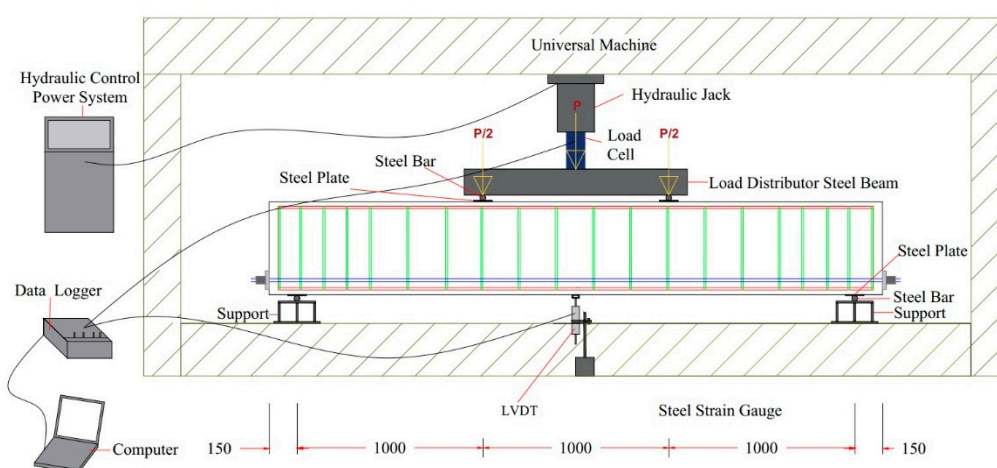


Figure 9. Diagram of tested specimens.

2.7. Experimental Procedure

Specimen were tested using the flexural testing rig (universal machine) subjected to the four-points load test system as shown in Figure 9. The procedures to operate the test machine are listed below:

1. The load cell and LVDTs were connected to the data logger to obtain the real time load, strains and displacement of the specimens as applied load increases see .

2. Connect the data logger to the computer. The data was automatically recorded and stored utilizing the computerized data acquisition system.
3. Loosen the load adjustment control wheel as to prevent any sudden application of load to the specimen.
4. Slowly and steadily tighten the load adjustment control wheel after the specimen is placed properly on the testing rig specimens were loaded.
5. The load control method was used during the test, the load was applied at an average rate of 90 kN/min during the linear elastic stage. As the cracks developed and, thus, the concrete had a plastic behavior, the digital load indicator was not showing a constant loading rate anymore.
6. Because of the safety concern, the test was terminated when the specimens remind in a state where the load would be remain constant or slightly decrease and when the displacement was significantly increased. The tests was take an average period of 16 minute from beginning of loading process until the test was terminated.
7. Hold the load adjustment control wheel and highlight the crack with line and mark each of the crack.
8. Loosen the load adjustment control wheel before turning of the machine and disconnect if from the computer.

3. Expemental Results and Discusions

3.1. Tested Specimens

All specimens have same cross section and reinforcenmt rebar details but they have different tendon profile layout.

A total of ten unbounded post-tensioned prestressed beams were tested under four point loading test. Load-deflection curves, crack patterns and modes of failures are used used to investigate flexture behavior of prestressed bridge girders.

3.2. Load-Deflection Curves

Based on the result of the four points load test, the load-deflection curves of mid-span of each beam were obtained. The load and corresponding deflection at first cracking load and ultimate load for all beams are listed in Table 4.

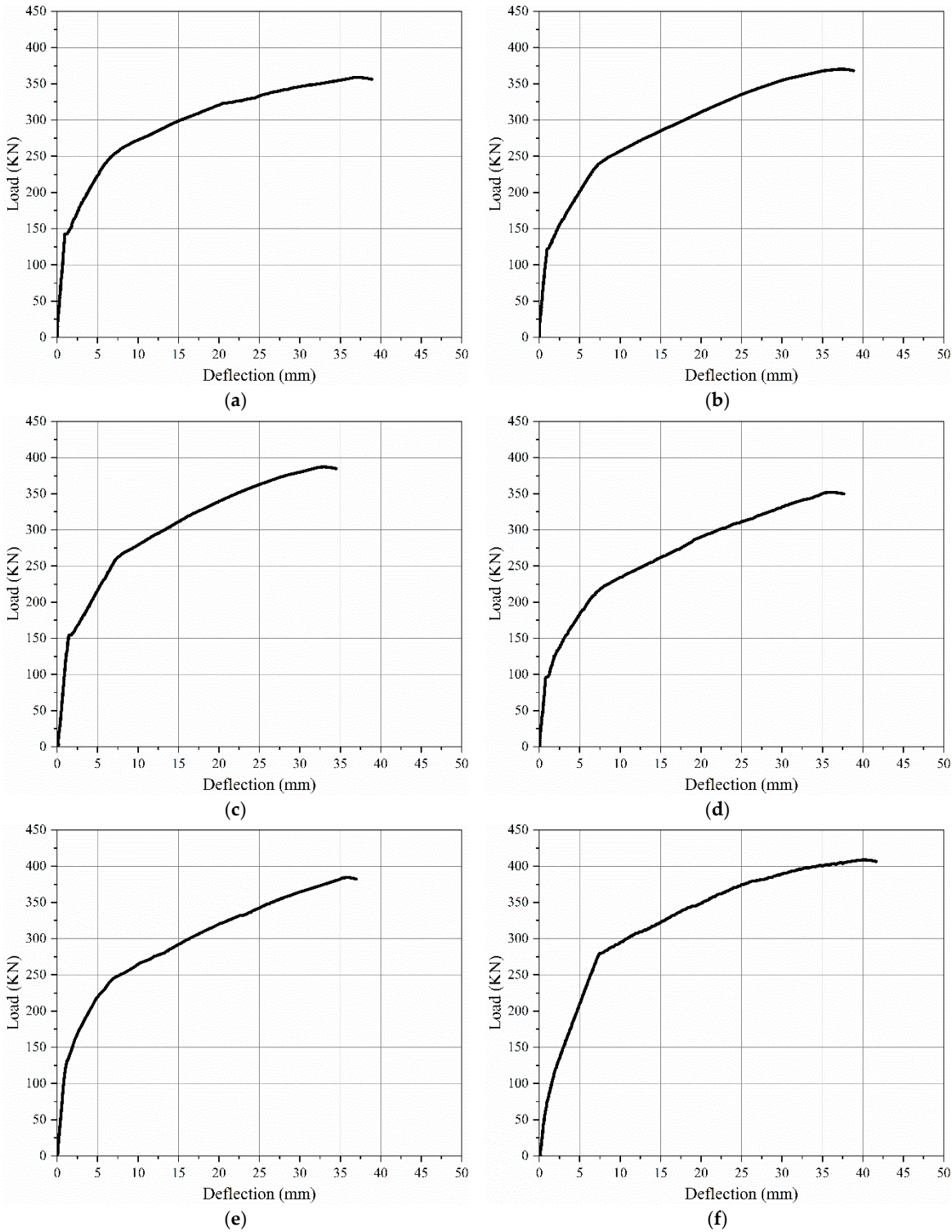
Table 4. Summary of expement result.

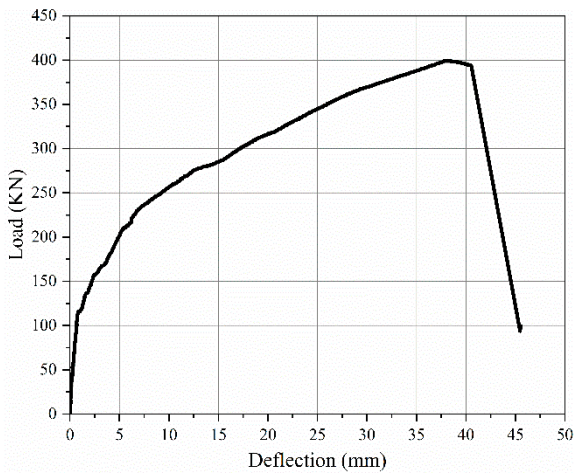
Specimen Name	First Crack Load (KN)	First Crack Deflection (mm)	Ultimate Load (KN)	Ultimate Load Deflection (mm)	P_{cr}/P_u %	Failure Mode
	P_{CR}	Δ_{CR}	P_u	Δ_u		
GF-1 ST	142.60	0.95	358.70	36.80	39.75%	Flexural ^{a,b}
GF-2 TR	122.02	0.96	371.63	36.76	32.83%	Flexural ^{a,b}
GF-3 TR	154.12	1.42	386.72	32.36	39.85%	Flexural ^{a,b}
GF-4 TR	95.80	0.79	351.27	35.24	27.27%	Flexural ^{a,b}
GF-5 PR	131.72	1.16	383.75	35.22	34.32%	Flexural ^{a,b}
GF-6 PR	80.00	1.11	408.30	39.56	19.59%	Flexural ^{a,b}
GF-7 PR	119.1	0.85	398.98	37.83	29.85%	Flexural ^{a,b}
GF-1 HA	150.45	1.52	426	35.74	35.32%	Flexural ^{a,b}
GF-2 HA	151.03	1.20	434.00	35.00	34.80%	Flexural ^{a,b}
GF-3 HA	139.02	1.20	409.00	37.90	33.99%	Flexural ^{a,b}

^a Yielding of tension reinforcement. ^b Large opening of flexural crack.

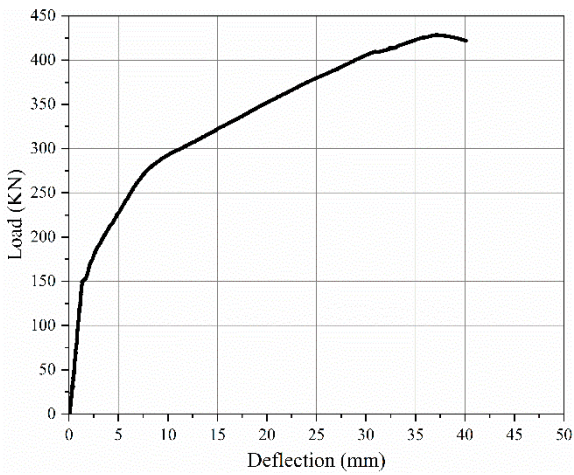
Generally, all specimens exhibited a linear response before cracking. Then, with the increase of the applied load, the ratio of the load to mid-span deflection decreased, that means the stiffness of

tested beams decreased. Consequently, a plastic response was noted due to the yielding of the longitudinal tension reinforcement, which lasted until the end of the test, as shown in Figure 10.

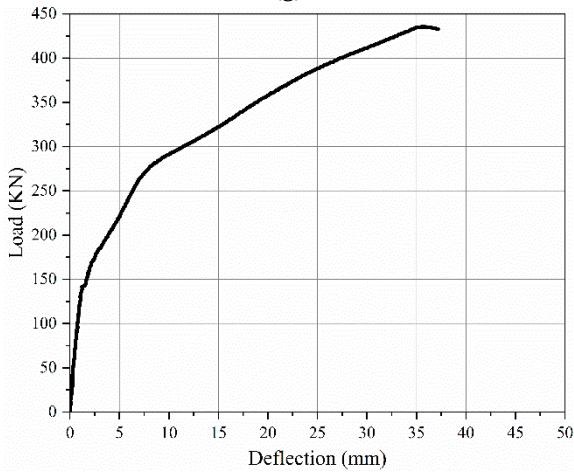




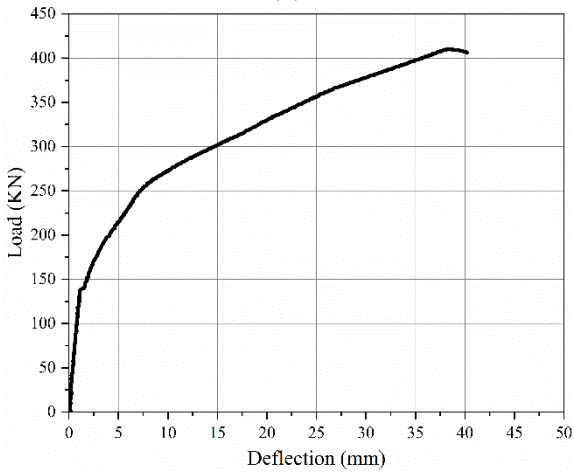
(g)



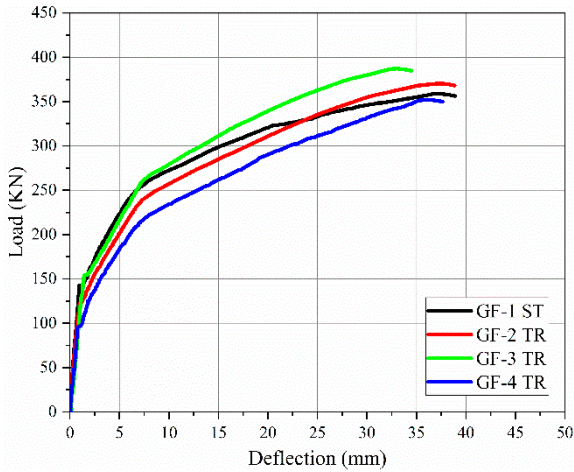
(h)



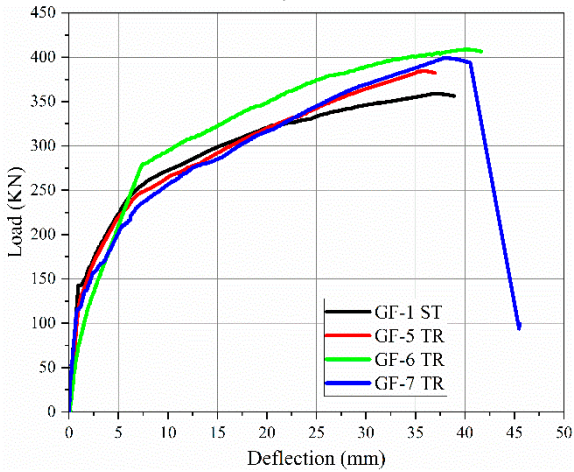
(i)



(j)



(k)



(l)

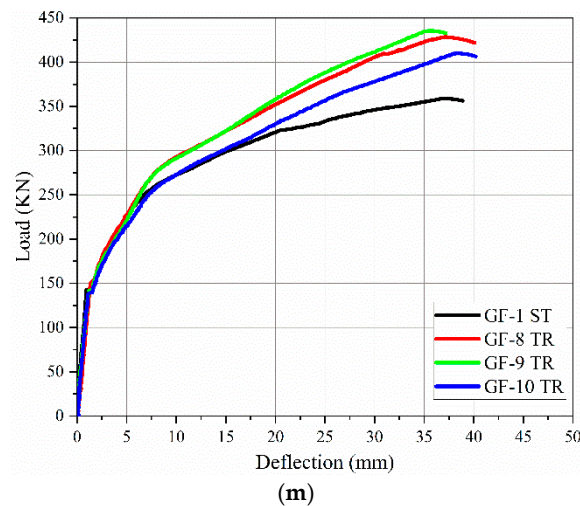


Figure 10. Load-deflection curves: (a) GF-1 ST. (b) GF-2 TR. (c) GF-3 TR. (d) GF-4 TR. (e) GF-5 PR. (f) GF-6 PR. (g) GF-7 PR. (h) GF-1 HA. (i) GF-2 HA. (j) GF-3HA. (k) GF-1 ST, GF-2 TR, GF-3 TR and GF-4 TR. (l) GF-1 ST, GF-5 TR, GF-6 TR and GF-7 TR. (m) GF-1 ST, GF-8 TR, GF-9 TR and GF-10 TR.

As observed in Figure 10 (a), the load-deflection curve for the control specimen (GF-1 ST) with straight tendon profile layout, it exhibited linear response before cracking (Elastic Stage) in which load varies linearly with deflection, as the load continues to increase, the first cracks appear in the concrete at 142.60 kN and deflection 0.95 mm. This marks the transition from elastic to inelastic behavior (Elastic-Plastic stage), the slope of the load-deflection curve gradually decrease this mean the deflection increase faster than the load due to decrease in stiffness resulted from cracking. As load increased a new inflection point was found in load-deflection curve (the slope of the load-deflection curve gradually decreased a gain). Then a plastic response (Plastic Stage) was observed due to yielding of longitudinal tension reinforcement until the test was finished. In this stage the load-deflection curve tends to be horizontal ,while the load no longer raises and deflection increase sharply. The ultimate load (maximum load) was 358.70 kN and deflection was 36.80 mm.

For the specimen GF-2 TR with trapezoidal tendon profile and eccentricity at end (anchorage point of the tendon) $e_e = +80$ mm, the load-deflection curve as observed in Figure 10 (b), although, its elastic stage less than the control beam, the first crack was appeared in the concrete at 122.02 kN and deflection 0.96 mm but it have higher ultimate load 371.63 kN and smaller deflection 36.76 mm at ultimate load. That means increasing in ultimate load by 12.93 kN with increasing rate 4% and decreasing in ultimate load deflection by 0.04 mm with increasing rate 0.11% as shown in Table 5.

Table 5. Comparison of ultimate load and ultimate load deflection of control beam with other specimens.

Compared Specimen	Increase in Ultimate Load		Decrease in Ultimate Load		Increase In Ultimate Load Deflection		Decrease In Ultimate Load Deflection	
	(kN)	%	(kN)	%	(mm)	%	(mm)	%
GF-1 ST & GF-2 TR	12.93	3.60%	-	-	-	-	0.04	0.11%
GF-1 ST & GF-3 TR	28.02	7.81%	-	-	-	-	4.44	12.07%
GF-1 ST & GF-4 TR	-	-	7.43	2.07%	-	-	1.56	4.24%
GF-1 ST & GF-5 PR	25.05	6.98%	-	-	-	-	1.58	4.29%
GF-1 ST & GF-6 PR	49.6	13.83%	-	-	2.76	7.50%	-	-
GF-1 ST & GF-7 PR	40.28	11.23%	-	-	1.03	2.80%	-	-
GF-1 ST & GF-1 HA	67.3	18.76%	-	-	-	-	1.06	2.88%
GF-1 ST & GF-2 HA	75.3	20.99%	-	-	-	-	1.8	4.89%
GF-1 ST & GF-3 HA	50.3	14.02%	-	-	1.1	3%	-	-

For specimen GF-3 TR with trapezoidal tendon profile layout and eccentricity at end (e_e) = 0, the load-deflection curve as observed in Figure 10 (c), its elastic stage greater than the control beam, the first crack was appeared in the concrete at 154.12 KN and deflection 1.42 mm. It have a higher ultimate load 386.72 KN and smaller deflection 32.36 mm at ultimate load. That means increasing in ultimate load by 28.02 KN with increasing rate 8% and decreasing in ultimate load deflection by 4.44 mm with decreasing rate 12.07% as shown in Table 5.

For specimen GF- 4 TR with trapezoidal tendon profile layout and eccentricity at end (e_e) = - 80 mm, the load-deflection curve as observed in Figure 10 (d), its elastic stage less than the control beam, the first cracks was appeared in the concrete at 95.80 KN and deflection 0.79 mm. It have a lower ultimate load 351.27 KN and smaller deflection 35.24 mm at ultimate load. That means decreasing in ultimate load by 7.43 KN with decreasing rate 2.07 % and decreasing in ultimate load deflection by 1.56 mm with decreasing rate 4.24% as shown in Table 5.

For the specimen GF-5 PR with parabolic tendon profile layout and eccentricity at end (e_e) = +80 mm, the load-deflection curve as observed in Figure 10 (e). Its elastic stage less than the control beam. Although, the first cracks was appeared in the concrete at 131.72 KN that was lesser than control beam and deflection 1.16 mm greater than the control beam but it have a higher ultimate load 383.75 KN and smaller deflection 35.22 mm at ultimate load. That means increasing in ultimate load by 25.05 KN with increasing rate 6.98% and decreasing in ultimate load deflection by 1.58 mm with decreasing rate 4.29% as shown in Table 5.

For specimen GF-6 PR with parabolic tendon profile layout and eccentricity at end (e_e) = 0, the load-deflection curve was observed in Figure 10 (f) although , its elastic stage lesser than the control beam, the first cracks was appeared in the concrete at 80 KN and deflection 1.11 mm but it have a higher ultimate load 408.3 KN and larger deflection 39.56 mm at ultimate load. That means increasing in ultimate load by 49.6 KN with increasing rate 13.83% and increasing in ultimate load deflection by 2.76 mm with increasing rate 7.50% as shown in Table 5.

For specimen GF-7 PR with parabolic tendon profile layout and eccentricity at end (e_e) = -80 mm, the load-deflection curve as observed in figure 10 (g), its elastic stage less than the control beam, the first crack was appeared in the concrete at 119.1 KN and deflection 0.85 mm. It have a higher ultimate load 398.98 KN and larger deflection 37.83 mm at ultimate load. That means increasing in ultimate load by 40.28 KN with increasing rate 11.23% and increasing in ultimate load deflection by 1.03 mm with increasing rate 2.88% as shown in Table 5.

For the specimens GF-1 HA with harped tendon profile layout and eccentricity at end (e_e) = +80 mm, the load-deflection curve as observed in Figure 10 (h), its elastic stage less than the control beam, the first crack was appeared in the concrete at 150.45 KN and deflection 1.52 mm. It have a higher ultimate load 426.00 KN and smaller deflection 35.74 mm at ultimate load. That means increasing in ultimate load by 67.3 KN with increasing rate 18.76% and increasing in ultimate load deflection by 1.06 mm with increasing rate 2.88% as shown in Table 5.

For specimen GF-2 HA with harped tendon profile layout and eccentricity at end (e_e) = 0, the load-deflection curve as observed in Figure 10 (i), its elastic stage larger than the control beam, the first crack was appeared in the concrete at 151.03 KN and deflection 1.20 mm. It have a higher ultimate load 434 KN but lower deflection 35.00 mm at ultimate load. That means increasing in ultimate load by 75.3 KN with increasing rate 20.99% and increasing in ultimate load deflection by 1.8 mm with increasing rate 4.89% as shown in Table 5.

For specimen GF-3 HA with harped tendon profile layout and eccentricity at end (e_e) = -80 mm, the load-deflection curve as observed in Figure 10 (j) although, its elastic stage less than the control beam, the first cracks was appeared in the concrete at 139.02 KN and deflection 1.20 mm and it showed a higher ultimate load 409.00 KN and greater deflection 37.90 mm at ultimate load. That means increasing in ultimate load by 50.3 KN with increasing rate 14.02% and increasing in ultimate load deflection by 1.1 mm with increasing rate 3% as shown in Table 5.

In the summary of comparison of the all specimens with the control beam as as illustrated in Figure 10 (k, l, m), the variation in ultimate loads and deflections at the ultimate loads were resulted

from the effect of tendon profile layout (trapezoidal, parabolic, harped) and end anchorage of tendons. Since the bending moment at every section is the product of the prestressing force and eccentricity, the beams with zero eccentricity of tendon profile layout at the end anchorages showed larger capacity from beams with end eccentricity because beams with zero eccentricity had a uniform compression stresses only without any tension stresses at supports and the distribution of applied load on the cross-section would be uniform in comparison with eccentric ones.

3.3. Crack Patterns and Mode of Failure

The cracking loads of each specimen were recorded during testing as soon as the first vertical cracks appeared. First crack appeared in bottom flange for all specimens. In some cases, specimens already had fine surface cracks before the test began, likely caused by drying shrinkage. These initial cracks often weren't visible until they had extended to the beam's surface. Additionally, some cracks were so small that they took time to become noticeable. As a result, the recorded cracking load was typically slightly higher than the actual cracking load.

The crack patterns and failure mode of the each specimens are shown in Figure 11 and Table 4. Flexural cracking was observed in all specimens in pure moment region initially appeared at the bottom flange of the girder between the two loading points. As the load continued to increase, the flexural crack propagate vertically upward, expanded and more crack would appear in constant moment region. Then some oblique flexural crack would propagate from bottom flange towered loading points. Finally, a reduction of loading capacity (beam stiffness) was noted resulting from cracks expanding and extending.

For specimens GF-1 ST, GF-2 TR, GF-3 TR, GF-4 PR and GF-5 PR the first crack was observed near mid-span. More cracks would appeared with increasing the applied load finally the first crack would be the major at the end of loading. For specimens GF-6 PR, GF-7 PR, GF-1 HA, GF-2 HA AND GF-3 HA the first crack was observed near mid-span. More cracks would propagate with increasing the applied load. Finally one of the propagated cracks near the left point loading would be the major crack at the end of the loading.

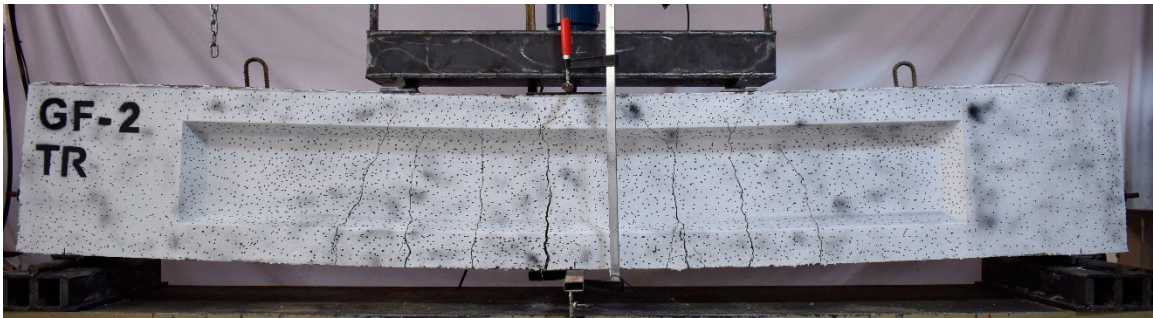
This means if the tendon profile layout at pure moment region was straight the final major crack would be near the mid-span. The final major crack position transfer to be near the left point load with increasing the tendon curvature for parabolic tendon profiles and the tendon slop for harped tendon profile.

For trapezoidal tendon profile, the major final crack would still near the mid-span of the beam because the tendon profile between the two point load was straight.

For parabolic tendon profile, GF-5 PR the major final crack would be near the midspan of the beam because the tendon curvature was very little between the two point load was straight. with increasing the tendon curvature for parabolic tendon profiles for GF-6 PR and GF-7 PR. The final major crack position transfer to be near the left point load.



(a)



(b)



(c)



(d)



(e)



(f)

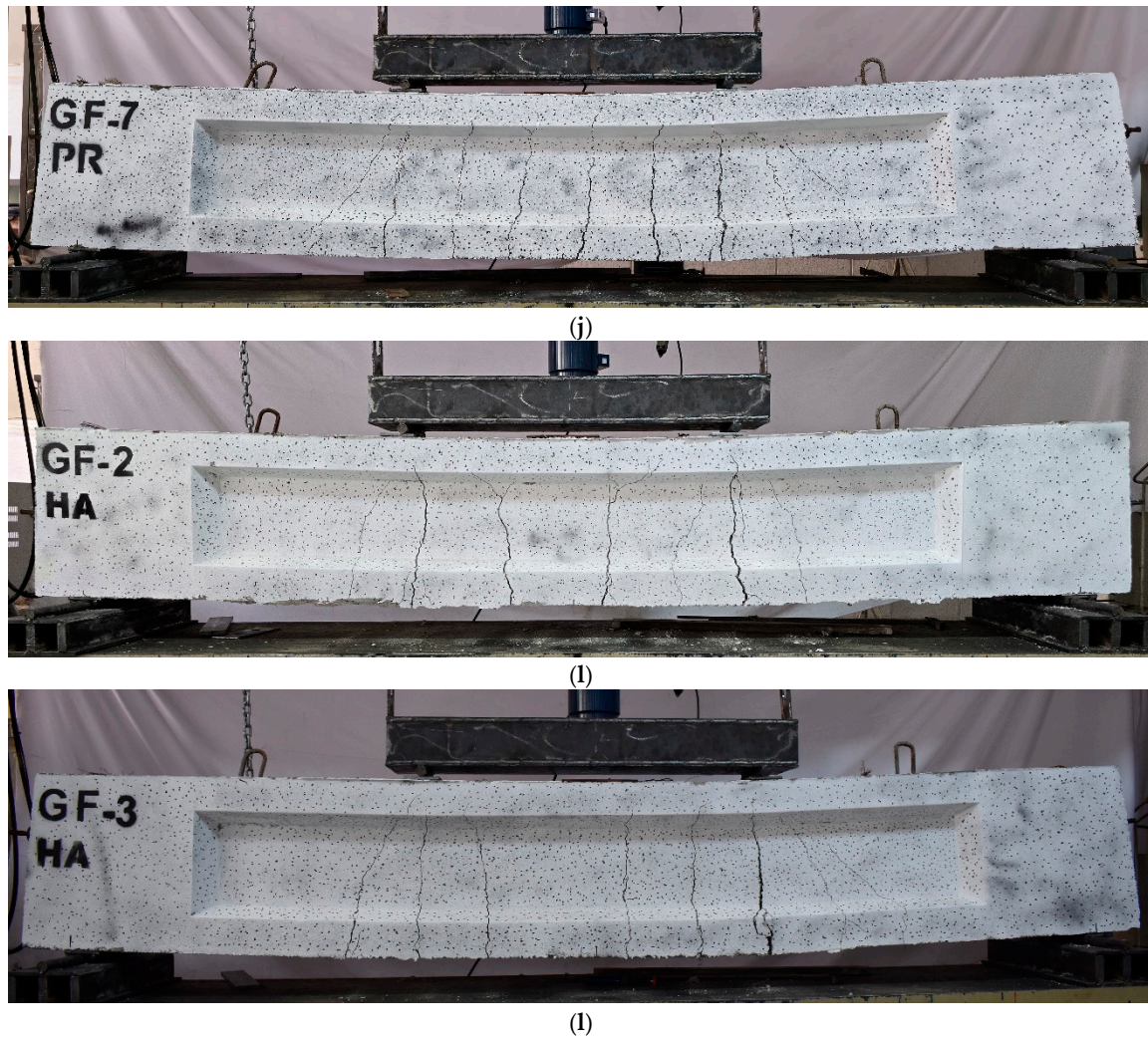


Figure 11. Crack pattern for tested specimens: (a) GF-1 ST, (b) GF-2 TR, (c) GF-3 TR, (d) GF-4 TR. (e) GF-5 PR. (f) GF-6 PR. (g) GF-7 PR. (h) GF-1 HA. (i) GF-2 HA. (j) GF-3HA.

4. Conclusion

In order to examine the effect of tendon profile layout on flexural strength of unbounded prestress concrete bridge I-girders, an experimental investigation was conducted on ten unbounded prestress concrete bridge I-girders with different tendon profile layout. The following conclusions were drawn from this study :-

1. The flexural destruction of unbounded prestress concrete bridge i-girders experience elastic, elastic-plastic and ductility stages, similar to bounded prestress concrete bridge i-girders. Unbounded prestress concrete bridge I-girder present superior ductility and deformation-recovery ability after unloading.
2. The tendon profile layout has a significant influence on the destruction process in unbounded prestress concrete bridge I-girders.
3. The experimental results showed that the flexural behavior of tested specimens is divided in to three stages: elastic stage, elastic-plastic stage and plastic stage. All specimens exhibit flexural failure.
4. The ultimate load of specimens using trapezoidal tendon profile, showed a maximum increased by 28.02 KN with increasing rate 7.81% for the specimen GF-3 TR if we compared it with control beam.
5. The ultimate load of specimens using parabolic tendon profile had maximum increased by 49.6 KN with increasing rate 13.83% for the specimen GF-6 PR if we compared it with control beam.

6. The ultimate load of specimens using harped tendon profile had maximum increased by 75.3 KN with increasing rate 20.99% for the specimen GF-2 HA if we compared it with control beam.
7. The deflection of specimens using trapezoidal tendon profile, the specimen GF-3 TR had minimum vertical deflection 32.36 mm, which lesser than control beam by 4.44 mm with decreasing rate 12.07 % from control beam.
8. The deflection of specimens using parabolic tendon profile, the specimen GF-5 PR had minimum vertical deflection 35.22 mm, which lesser than control beam by 1.58 mm with decreasing rate 4.29 % from control beam.
9. The deflection of specimens using parabolic tendon profile, the specimen GF-2 HA had minimum vertical deflection 35 mm, which lesser than control beam by 1.80 mm with decreasing rate 4.89 % from control beam.
10. Each tendon profiles shapes (trapezoidal, parabolic, harped) with eccentricity at end (e_e)=0, had maximum ultimate load capacity. It's can be concluded that specimen GF-9 HA with harped tendon profile had maximum ultimate load capacity from all other specimens. Also it's can be concluded that specimen GF-3 TR with trapezoidal tendon profile had minimum deflection from all other specimens which agree with the result of finite element analysis by Ansys and Sap software, that done by Dixit and Naser[27,28]. These enhancement in specimens stiffness, ultimate loads capacities and deflections because of effect of tendon profile layout on flexural capacity of girders.
11. The experimental results of tests on girders with optimized tendon profiles illustrated remarkable improvements in performance. These girders carried higher loads with less deflection than control beam. The efficiency of prestressing forces throughout the girder length makes the girders with optimized tendon configurations more performant. This allows for a more even distribution of the induced stresses to the concrete member, engaging more of the cross section for load carrying. This uniform stress distribution enhances ductility of the girder and hence the service life of the structure.

Author Contributions: Conceptualization, S.H. and O.A.; methodology, S.H.; validation, S.H., O.A. and A.L.; formal analysis, S.H.; investigation, S.H.; resources, S.H.; data curation, S.H.; writing—original draft preparation, S.H.; writing—review and editing, A.L and O.A.; visualization, S.H. , A.L. ; supervision, A.L. and O.A.; project administration, A.L. and O.A.

Funding: This research received no external funding.

Institutional Review Board Statement: Not applicable.

Informed Consent Statement: Not applicable.

Data Availability Statement: All data generated or analyzed during this study are available from the first author (Swar I. Hasib) on reasonable request.

Acknowledgments: The authors would like to acknowledge the Laboratory of Civil Engineering at the University of Salaheddin-Erbil for providing the facilities and resources required to conduct the experimental tests. Special thanks to the technical staff for their assistance and support throughout the research process. I extend my sincere gratitude to Kirkuk Limited Company for Concrete Girder for their expert technical support in the post-tensioning of beams. Special thanks to their skilled prestressing concrete plant staff, whose precision and professionalism were essential to this research.

Conflicts of Interest: The authors declare no conflict of interest.

References

1. Arthur H. Nilson *Design of Prestressed Concrete*; Second Edition.; 1987;
2. Naser, A.F.; Zonglin, W. Strengthening of Jiamusi Pre-Stressed Concrete Highway Bridge by Using External Post-Tensioning Technology in China. *Journal of Engineering and Applied Sciences* **2010**, *5*.

3. Naser, A.F.; Zonglin, W. Finite Element and Experimental Analysis and Evaluation of Static and Dynamic Responses of Oblique Pre-Stressed Concrete Box Girder Bridge. *Research Journal of Applied Sciences, Engineering and Technology* **2013**, *6*, doi:10.19026/rjaset.6.3572.
4. Abdullah, A.B.M.; Rice, J.A.; Hamilton, H.R.; Consolazio, G.R. Damage Identification in Unbonded Tendons for Post-Tensioned Bridges. In Proceedings of the International Conference on Advances in Experimental Structural Engineering; August 2015; Vol. 2015-August.
5. John Corven; Clay Naito; Stephen Pessiki *Designing and Detailing Post-Tensioned Bridges to Accommodate Nondestructive Evaluation*; 2018;
6. Nusrath Fahmeen.R; Satheesh V.S; Manigandan.M An Overview on Tendon Layout for Prestressed Concrete Beams. *IJISSET-International Journal of Innovative Science, Engineering & Technology* **2015**, *2*.
7. Lim, S.S.; Wong, J.Y.; Yip, C.C.; Pang, J.W. Flexural Strength Test on New Profiled Composite Slab System. *Case Studies in Construction Materials* **2021**, *15*, doi:10.1016/j.cscm.2021.e00638.
8. Tang, C.; Zhang, G.; Song, C.; Li, X.; Hou, Y. Flexural Behavior of Unbonded Prestressed Concrete Bridge Girders. *Advances in Civil Engineering* **2021**, *2021*, doi:10.1155/2021/6642513.
9. Moreira, L.S.; Sousa, J.B.M.; Parente, E. Nonlinear Finite Element Simulation of Unbonded Prestressed Concrete Beams. *Eng Struct* **2018**, *170*, doi:10.1016/j.engstruct.2018.05.077.
10. Pérez, P.M.; Sensale, B. Improved Prediction of Long-Term Prestress Loss in Unbonded Prestressed Concrete Members. *Eng Struct* **2018**, *174*, doi:10.1016/j.engstruct.2018.07.038.
11. ACI 318-19 Building Code Requirements for Structural Concrete (ACI 318-19) Commentary on Building Code Requirements for Structural Concrete (ACI 318-19). *American Concrete Institute* **2019**.
12. AASHTO *AASHTO LRFD Bridge Design Specifications: SI Unit 4th Edition 2007*; 2007;
13. Kim, M.S.; Lee, Y.H. Flexural Behavior of Posttensioned Concrete Beams with Unbonded High-Strength Strands. *Advances in Materials Science and Engineering* **2020**, *2020*, doi:10.1155/2020/5317456.
14. Najem, R.M. Optimum Tendon Placement for Post Tensioned S.S. Beam with Variable Eccentricity. *Tikrit Journal of Engineering Sciences* **2018**, *25*, doi:10.25130/tjes.25.1.05.
15. Park, H.; Jeong, S.; Lee, S.C.; Cho, J.Y. Flexural Behavior of Post-Tensioned Prestressed Concrete Girders with High-Strength Strands. *Eng Struct* **2016**, *112*, doi:10.1016/j.engstruct.2016.01.004.
16. Dogu, M.; Menkulasi, F. A Flexural Design Methodology for UHPC Beams Posttensioned with Unbonded Tendons. *Eng Struct* **2020**, *207*, doi:10.1016/j.engstruct.2020.110193.
17. Oukaili, N.; Peera, I. Behavioral Nonlinear Modeling of Prestressed Concrete Flexural Members with Internally Unbonded Steel Strands. *Results in Engineering* **2022**, *14*, doi:10.1016/j.rineng.2022.100411.
18. Vichare, A.M.; Barbudhe, P.S.; Rele, R. Effective Positioning of Cable Profiles in Prestressed: I Girders. *J Emerg Technol Innov Res* **2024**, *11*.
19. Aravinthan, T.; Witchukreangkrai, E.; Mutsuyoshi, H. Flexural Behavior of Two-Span Continuous Prestressed Concrete Girders with Highly Eccentric External Tendons. *ACI Struct J* **2005**, *102*, doi:10.14359/14411.
20. Ibrahim, R.K.; Lateef, A.M. Flexural Behavior of Corroded One-Way Slabs Strengthened with CFRP in Two Different Techniques. *Innovative Infrastructure Solutions* **2024**, *9*, doi:10.1007/s41062-024-01648-6.
21. Khalid Khdir, M.; Qziz, O.Q. ZANCO Journal of Pure and Applied Sciences The Flexural Behavior of UHP Pre-Stressed Concrete Beams. *Zanco J Pure Appl Sci* **2016**.
22. Burhan, M. A FINITE ELEMENT MODEL FOR THE STUDY OF THE CREEP AND SHRINKAGE EFFECTS IN THE PARTIALLY PRESTRESSED CONTINUOUS COMPOSITE BEAMS. *Tikrit Journal of Engineering Sciences* **2005**, *12*, doi:10.25130/tjes.12.1.07.
23. Ng, P.L.; Kwan, A.K.H. Practical Determination of Prestress Tendon Profile by Load-Balancing Method. *HKIE Transactions Hong Kong Institution of Engineers* **2006**, *13*, doi:10.1080/1023697X.2006.10668050.
24. Ahmad Ali Khan; K.K.Pathak; N.Dindorkar CABLE LAYOUT DESIGN OF ONE WAY PRESTRESSED SLABS USING FEM. *Journal of Engineering, Science and Management Education* **2010**, *2*.
25. Chaitanya Kumar J.D; Lute Venkat Genetic Algorithm Based Optimum Design of Prestressed Concrete Beam. *International Journal for Computational Civil and Structural Engineering* **2013**, *3*, doi:10.6088/ijcser.2.
26. Colajanni, P.; Recupero, A.; Spinella, N. Design Procedure for Prestressed Concrete Beams. *Computers and Concrete* **2014**, *13*, doi:10.12989/cac.2014.13.2.235.

27. Dixit, A.S.; Khurd, V.G. Effect of Prestressing Force, Cable Profile and Eccentricity on Post Tensioned Beam. *International Research Journal of Engineering and Technology* **2017**, *4*.
28. Naser, A.F. Optimum Design of Vertical Steel Tendons Profile Layout of Post-Tensioning Concrete Bridges: Fem Static Analysis. *ARPJ Journal of Engineering and Applied Sciences* **2018**, *13*.
29. Mohammed, A.H.; Abdul-Razzaq, K.S.; Mohammedali, T.K.; Nassani K., D.E.; Hussein, A.K. Finite Element Modeling of Post-Tensioned Two-Way Concrete Slabs under Flexural Loading. *Civil Engineering Journal* **2018**, *4*, doi:10.28991/cej-030964.
30. Zelickman, Y.; Amir, O. Layout Optimization of Post-Tensioned Cables in Concrete Slabs. *Structural and Multidisciplinary Optimization* **2021**, *63*, doi:10.1007/s00158-020-02790-2.
31. Xu, G.; Zeng, M.; Su, Q. Layout and Optimization of the External Prestressing Tendons of Hybrid Beam Rigid Frame Bridges. In Proceedings of the IOP Conference Series: Earth and Environmental Science; 2021; Vol. 719.
32. Usha Rani, M. Effect of Tendon Profile on Deflections in Prestressed Concrete Beams Using C Programme. *International Journal of Computer Science and Engineering* **2021**, *8*, doi:10.14445/23488387/ijcse-v8i11p102.
33. Mohamed, G.A.; Eisa, A.S.; Purcz, P.; Ručinský, R.; El-Feky, M.H. Effect of External Tendon Profile on Improving Structural Performance of RC Beams. *Buildings* **2022**, *12*, doi:10.3390/buildings12060789.
34. Pavic, A. *Prestressed Concrete: A Fundamental Approach*; 2010; Vol. 5; ISBN 0136081509.
35. Arthur H. Nilson; David Darwin; Charles W. Dolan *Design of Concrete Structures*; 14th ed.; 2010;
36. ACI Committee 211 *Selecting Proportions for Normal-Density and High-Density Concrete-Guide Inch-Pound Units Selecting Proportions for Normal-Density and High-Density Concrete-Guide*; 2022;
37. Othman S. Hassan *Concrete Job Mix Formula for (Precast-Prestressed Girder Plant) Kirkuk Limited Company for Concrete Girder*; kirkuk, 2023;
38. ASTM C496/C496M-17 Standard Test Method for Splitting Tensile Strength of Cylindrical Concrete Specimens. *ASTM Standard Book* **2017**.
39. American Society for Testing and Materials (ASTM) Astm C78/C78M -18 Standard Test Method for Static Modulus of Elasticity and Poisson's Ratio of Concrete in Compression. *Standard Test Method for Flexural Strength of Concrete (Using Simple Beam with Third-Point Loading)*ASTM International. USA **2002**, 04.02.
40. American Standard Testing and Material ASTM C469 Standard Test Method for Static Modulus of Elasticity and Poisson's Ratio of Concrete in Compression. *ASTM Standard* **2014**, 04.

Disclaimer/Publisher's Note: The statements, opinions and data contained in all publications are solely those of the individual author(s) and contributor(s) and not of MDPI and/or the editor(s). MDPI and/or the editor(s) disclaim responsibility for any injury to people or property resulting from any ideas, methods, instructions or products referred to in the content.